

## Article

# Preparation and Corrosion Resistance of OMMT/EP Composite Coatings in Sulfur-Containing Sodium Aluminate Solution

Jun Xu <sup>1,2</sup>, Dongyu Li <sup>1,2</sup>, Hanli Wang <sup>1,2</sup> and Bianli Quan <sup>1,2,\*</sup><sup>1</sup> College of Materials and Metallurgy, Guizhou University, Guiyang 550025, China<sup>2</sup> Guizhou Province Key Laboratory of Metallurgical Engineering and Process Energy Saving, Guiyang 550025, China

\* Correspondence: bianli0901@163.com

**Abstract:** Organic montmorillonite (OMMT) was prepared from Na-montmorillonite (MMT) by Hexadecylamine (HDA) modification. The composite material has good smoothness, acidity, and salt resistance. OMMT was characterized using small-angle X-ray diffraction, Fourier transform infrared spectroscopy, scanning electron microscopy, and a video optical contact angle measuring instrument. The results showed that the layer spacing was enlarged from 1.44 nm to 2.87 nm after the modification, and the hydrophobicity performance was greatly improved. The organic modification of MMT was successful. The surface morphology, roughness, and anticorrosion properties of the organic montmorillonite/epoxy (OMMT/EP) composite coating were investigated and compared with those of the epoxy (EP) coating. The OMMT/EP composite coating had a flatter surface than the EP coating. The roughness was reduced from 65.5 nm to 10.3 nm. The electrochemical impedance spectroscopy showed that the composite coating's thickness positively affected its anticorrosion performance, the corrosion current density ( $I_{\text{corr}}$ ) decreased with the increase in thickness, and its maximum impedance was much larger than that of EP coating. The protection efficiency of the OMMT/EP composite coating was 77.90%, which is a significant improvement over the EP's 31.27%. In addition, the corrosion resistance of the composite coating gradually decreased with increasing immersion time, but the change was insignificant.

**Keywords:** montmorillonite; epoxy resin; Q235 steel; sodium aluminate solution; corrosion resistance

**Citation:** Xu, J.; Li, D.; Wang, H.; Quan, B. Preparation and Corrosion Resistance of OMMT/EP Composite Coatings in Sulfur-Containing Sodium Aluminate Solution. *Coatings* **2024**, *14*, 546. <https://doi.org/10.3390/coatings14050546>

Academic Editor: Alina Vladescu

Received: 29 February 2024

Revised: 20 April 2024

Accepted: 22 April 2024

Published: 27 April 2024



**Copyright:** © 2024 by the authors. Licensee MDPI, Basel, Switzerland. This article is an open access article distributed under the terms and conditions of the Creative Commons Attribution (CC BY) license (<https://creativecommons.org/licenses/by/4.0/>).

## 1. Introduction

The Bayer alumina production process is adversely affected by the accumulation of sulfur in the raw materials and production process [1,2], especially by the severe corrosion of steel equipment. Therefore, the surface protection of alumina production equipment is critical [3,4]. Polymer coatings have been widely used for the corrosion protection of metal substrates, and epoxy resin-based anticorrosion coatings are widely used due to their excellent adhesion resistance and other advantages [5–7]. However, the epoxy resin coatings form some voids and defects with the evaporation of solvents during the curing process, which have insufficient barrier properties against corrosive media, leading to the shortening of the corrosion path between the corrosive media and the surface of the substrate material, thus accelerating corrosion [8].

Incorporating nanomaterials with a shielding effect into epoxy resin coatings can enhance the corrosion resistance of the coatings by reducing the porosity and increasing the diffusion path of corrosive media [9,10]. Na-montmorillonite (MMT), as a two-dimensional nanomaterial, has a unique layered structure, large aspect ratio, and very high surface area and has been widely used by researchers in the field of coating and anticorrosion, but MMT has a small layer spacing and is prone to agglomeration, and it needs to be organically modified so that the performance of the MMT can be improved. Modification of MMT using quaternary alkyl ammonium salts [11], silane coupling agents [12], and

hyperbranched polymers HBPs [13] to improve interlayer spacing and dispersion resulted in improved mechanical properties and inhibition as well as environmental stability of the epoxy-based composite coatings [14]. The composite coatings incorporating modified MMT provided barrier corrosion protection to carbon steel in NaCl solution, blocking defects and reducing the transport of water and corrosive materials [15]. The organic montmorillonite/epoxy (OMMT/EP) composite coating was shown to have superior protective properties to those of the original epoxy coatings after the weight loss results, optical examination, and microscopic examination of samples. The anticorrosion effect of montmorillonite in epoxy resin was verified [16]. The incorporation of graphene oxide on the basis of OMMT allows for the preparation of a high-performance epoxy anticorrosion coating with a larger contact angle and a smoother surface than epoxy coatings [17]. The addition of different types of fillers to the epoxy resin base will play different roles. The new anticorrosive coating synthesized by doped polyaniline, reduced graphene oxide, and MMT showed superior anticorrosive performance of the synthesized nanocomposite according to the Tafel test, where the corrosion current of the synthesized nanocomposite was lower than that of other samples [18]. These composite coatings are often studied in seawater environments. However, the problem of corrosion in steel production equipment is also particularly common in the Bayer alumina production process, where the main corrosive medium is the sulfur-containing sodium aluminate solution, which results in an alkaline corrosion [19,20]. The corrosion of production equipment can cause economic losses and serious environmental pollution problems. Therefore, the corrosion resistance of composite coatings in this environment is worth exploring [21].

The main stages in the Bayer alumina production process are divided into four stages: bauxite dissolution, dilution of sodium aluminate solution, crystal species separation, and mother liquor evaporation. The mother liquor in the evaporation process contains  $S^{2-}$  and  $S_2O_3^{2-}$ , which is the main cause of corrosion in production equipment, so this experiment simulates the corrosion resistance of OMMT/EP composite coatings prepared in this corrosive environment. FTIR, XRD, SEM, and AFM were used to analyze the intercalation behavior, morphological changes, and hydrophobicity of organic montmorillonite (OMMT) with Hexadecylamine (HDA). The effect of OMMT on the surface roughness and morphology of the OMMT/EP composite coating was investigated by AFM and SEM. Polarization curves and electrochemical impedance spectroscopy reveal the corrosion resistance of the composite coating in corrosive media containing sodium sulfoaluminate.

## 2. Experiments

### 2.1. Experimental Materials

The following chemical reagents and materials were used directly without further treatment: Q235 steel (size 10 mm × 10 mm × 1 mm), 93 mmol/100 g of Na-montmorillonite (MMT, Guzhang Shanphosphorite Mineral Products Co., Ltd., Hunan, China), Hexadecylamine (HDA, Aladdin Reagent Co., Ltd., Shanghai, China), dodecyl benzene sulfonic acid (DBSA, Aladdin Reagent Co., Ltd., Shanghai, China), epoxy resin E44 (Nantong Xingxing Synthetic Materials Co., Ltd., Nantong, China), environmental protection diluent (Shanghai Kangquzhou Chemical Co., Ltd., Shanghai, China), acetone (Chongqing Chuandong Chemical Industry Group, Chongqing, China), and polyamide D-230 (Aladdin Reagent Company).

Q235 steel was 240-mesh, 400-mesh, 600-mesh, 800-mesh, 1000-mesh and 1200-mesh sandpaper for surface grinding and polishing, and then we used anhydrous ethanol and acetone ultrasonic cleaning, drying treatment, and placed it on standby.

### 2.2. Preparation of OMMT

Suspension A was prepared by dispersing MMT into 500 mL of deionized water. A certain amount of HDA, which was equivalent to 1.0 CEC of MMT, was added into 50 mL of absolute ethanol while stirring to obtain suspension B. Suspensions A and B were mixed in a water bath at 80 °C to obtain Suspension C. The precipitation was collected by centrifugation and washed with anhydrous ethanol and deionized water until there was

no precipitation in the waste liquid added to  $\text{AgNO}_3$ . Precipitate was dried and ground to obtain OMMT.

### 2.3. Preparation of OMMT/EP Composite Coating

The preparation of OMMT/EP composite coating and its role in the environment are shown in Figure 1. It is shown that MMT was modified by HDA and then intercalated into MMT layers to prepare organic modified filler (OMMT), and OMMT/EP composite coatings were obtained by adding OMMT filler into the epoxy resin base and fusing it. The measure of epoxy resin was diluted, OMMT powder was added, and the mixture was obtained by stirring at  $80\text{ }^\circ\text{C}$ . Then, polyamide D-230 and acetone (6:1 quality ratio) were added to form a mixed slurry of OMMT and epoxy resin, and the mixed slurry was covered on the surface of Q235 steel with a wire rod coater to form the OMMT/EP composite coating.

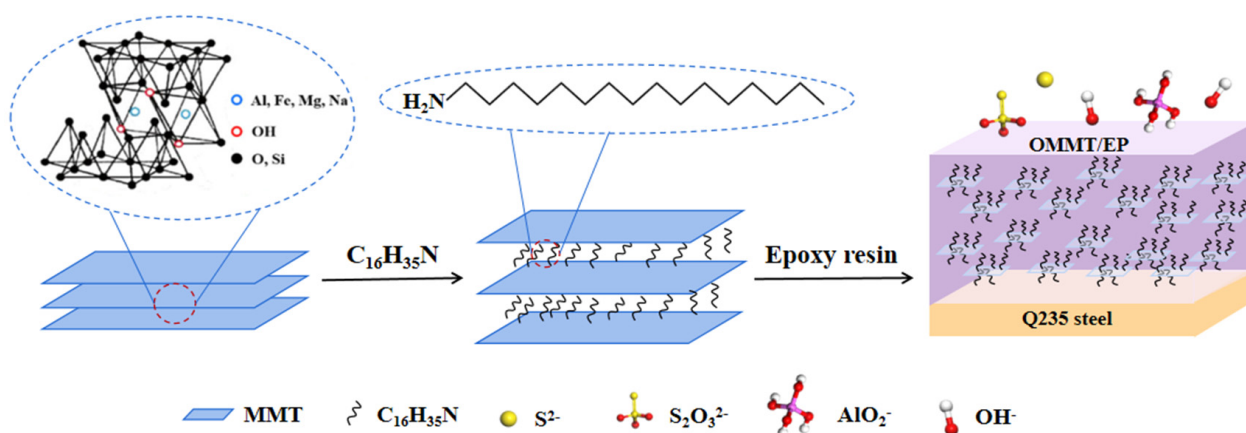


**Figure 1.** The preparation of OMMT/EP composite coating and its role in the environment.

### 2.4. Electrochemical Tests

The electrochemistry workstation of Shanghai Chenhua (CHI660E) was used for the electrochemical tests. In the tests, the corrosive environment was  $90\text{ }^\circ\text{C}$  in solutions of sodium aluminate containing  $5\text{ g/L S}^{2-}$  and  $5\text{ g/L S}_2\text{O}_3^{2-}$ ; a three-electrode system was used, with a platinum electrode as the auxiliary electrode, an OMMT/EP composite coating for the working electrode, and a saturated mercuric glycol electrode as the reference electrode. The test's potential range of polarization curve is  $-1.5\text{ V}\sim-1.05\text{ V}$ , and the scanning rate is  $3\text{ mV/s}$ . Electrochemical impedance spectroscopy (EIS) has a frequency range of  $0.01\text{--}10^5\text{ Hz}$  and an amplitude of  $5\text{ mV}$ .

### 2.5. Characterization Methods

The X-ray diffractometer (XRD UltimaIV, Rigaku, Tokyo, Japan) had an operating voltage of  $40\text{ kV}$ , a current of  $40\text{ mA}$ , and a scanning rate of  $1^\circ/\text{min}$  with  $\text{Cu K}\alpha$  as the incident light source. Fourier transform infrared spectroscopy (FTIR, Nicolet iS50, Thermo Field Company, Boston, MA, USA) was measured range from  $400\text{ to }4000\text{ cm}^{-1}$ . Scanning electron microscopy (SEM, Sigma300, ZEISS, Jena, Germany) was performed at  $15\text{ kV}$ . An atomic force microscope (AFM, Bruker Dimension ICON, Bruker, Billerica, MA, USA) determined the roughness of the coating surface. A video optical contact angle measuring instrument was also used (OCA, JY-82C, Chengde Dingsheng Company, Chengde, China).

## 3. Results and Discussion

### 3.1. Study on Properties of Modified MMT

Figure 2 shows the performance detection of OMMT. Figure 2a shows the infrared detection profile of MMT, HDA, and OMMT. The FT-IR plot of OMMT shows characteristic

peaks of HDA and MMT at  $2919\text{ cm}^{-1}$ ,  $2851\text{ cm}^{-1}$ ,  $1037\text{ cm}^{-1}$ , and  $798\text{ cm}^{-1}$ , respectively. Organic molecules displaced interlayer  $\text{Na}^+$ , resulting in OMMT. This indicates that combining the organic substance HDA and MMT was successful.

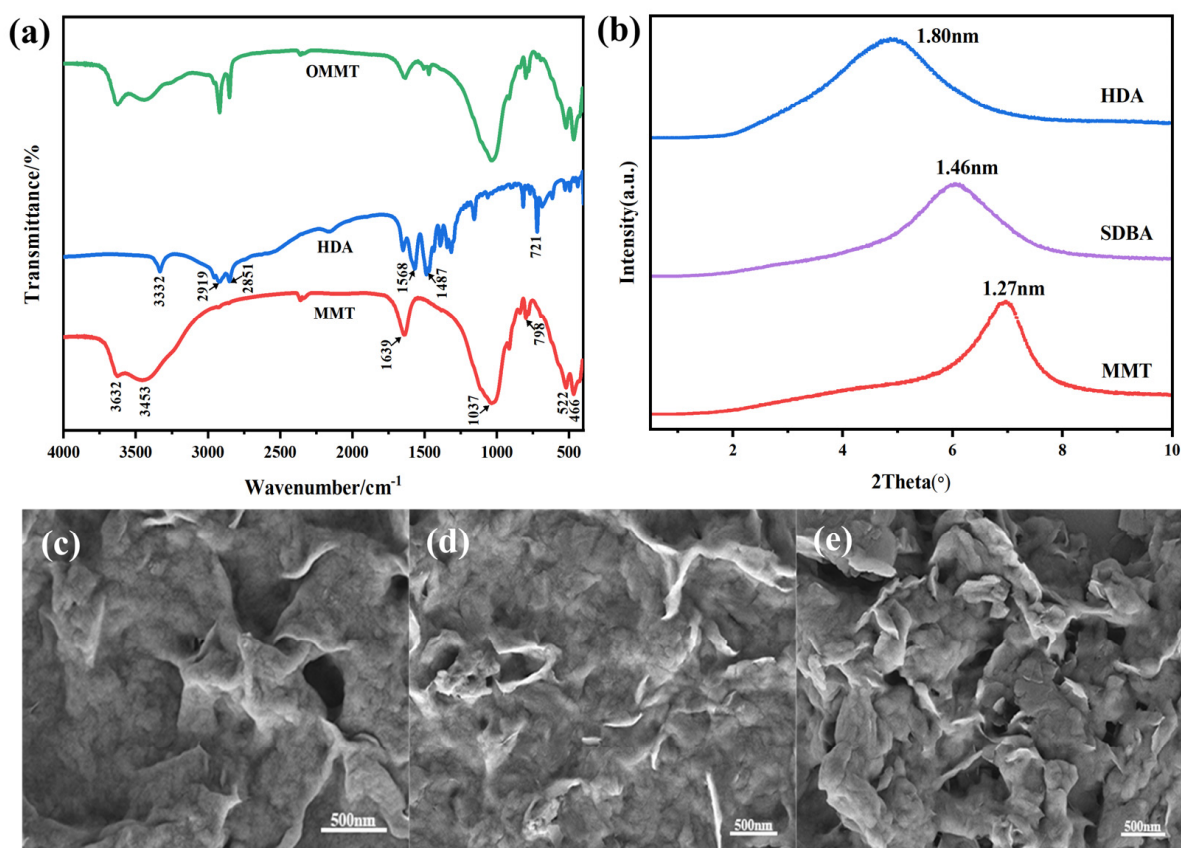


**Figure 2.** (a) FTIR spectroscopy of MMT, HDA, and OMMT; (b) XRD patterns of MMT, SDBA, and HDA; SEM plot of (c) MMT, (d) SDBA, and (e) HDA.

Figure 2b is the XRD plot of MMT and MMT after the organic modification of DBSA and HDA. The  $2\theta$  of the diffraction peaks on MMT's (001) face organically modified with DBSA and HDA were at  $6.05^\circ$  and  $4.91^\circ$ , respectively. The variation in layer spacing was calculated using Bragg's equation ( $2d\sin\theta = n\lambda$ ) and was found to be 1.27 nm, 1.46 nm, and 1.80 nm for MMT and MMT organically modified with DBSA and HDA, respectively. These results show that the HDA pretreatment increased the MMT interlayer spacing by 0.53 nm, facilitating the in situ intercalation of the MMT with the urushiol titanium polymer. The increase in the interlayer spacing of MMT obtained by HDA modification was large, so HDA-modified MMT was used as the filler in this experiment [22].

The limited dispersion of MMT layers can be seen in Figure 2c. The surface morphology of the MMT modified by adding anionic surfactant SDBA is shown in Figure 2d, and the layer dispersibility has not changed obviously. In Figure 2e, modified by the HDA, it shows significant changes in morphology, dispersion, and curling as well as more uniformity in the edges of the layer and its thickness [23]. The results show that HDA was successfully interpolated into the MMT interlayers rather than simply blended, and the results are consistent with the above FT-IR and XRD analyses.

### 3.2. Influence of HDA Content on MMT

XRD plots of the effect of the addition of different contents of HDA on the interlayer spacing are shown in Figure 3a. The layer spacing of the OMMT increases with increasing content as the content increases from 0.5 CEC to 1.5 CEC. As the organic content continues to increase, the interlayer spacing of the OMMT shows a tendency to decrease because too

much organic matter enters the interlayer of the MMT. When the content reaches 1.5 CEC, the  $2\theta$  of the diffraction peaks on the (001) surface are at  $2.90^\circ$  and  $6.21^\circ$ , respectively, and according to Bragg's equation  $2d\sin\theta = n\lambda$ , the layer spacing is obtained to be optimized at 2.87 nm and 1.46 nm, respectively [24].

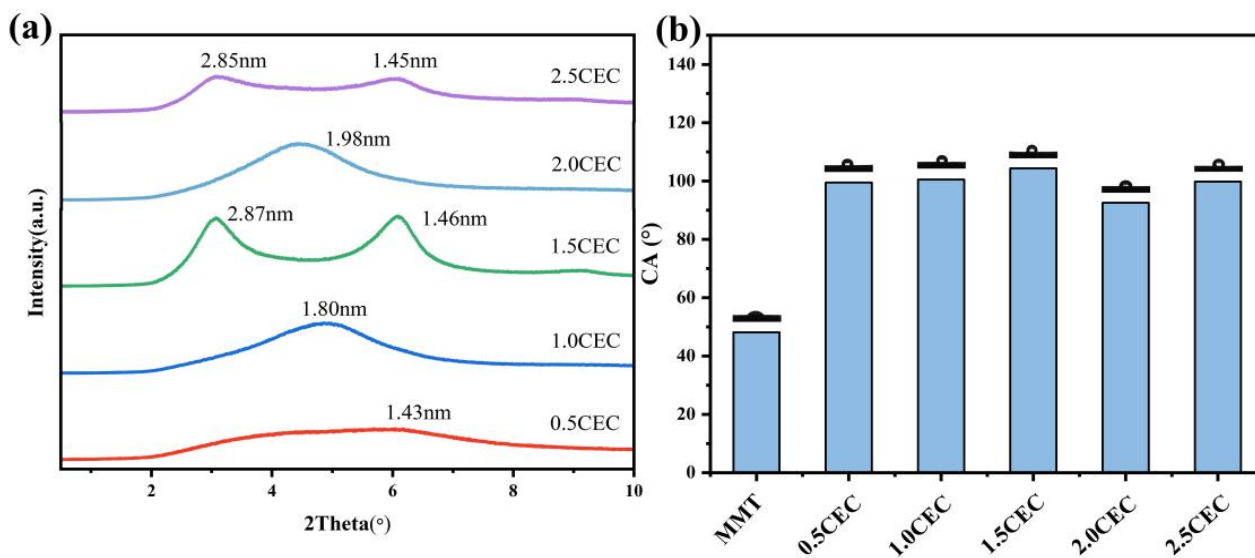


**Figure 3.** (a) XRD patterns of MMT modified with different HDA contents; (b) test chart of water contact angle of different HDA contents.

OCA was performed on MMT modified with HDA content, as shown in Figure 3b. The contact angle of the OMMT was significantly increased compared to that of the natural MMT. The contact angle was maximum when the organic content was 1.5 CEC, and the results indicated that the surface polarity of the OMMT changed, resulting in the hydrophilicity becoming hydrophobic, which provided an excellent basis for the final prepared composite coating.

### 3.3. Study on Properties of Modified OMMT/EP Composite Coating

The evaporation of solvents during the drying process of EP coating can lead to some voids and defects on the surface of the coating. The possible presence of hollows and depressions on the surface can be seen in Figure 4a. Combined with the AFM of the EP coating, the corrosive medium will come into contact with the Q235 steel substrate through these voids and defects, thus accelerating corrosion [25]. OMMT fillers were added to the epoxy resin at 3% and 7%, respectively, in combination with organic solvents to form the OMMT/EP composite coating. In Figure 4b,c, it can be seen that the pores and defects on the surface of the composite coating have been filled and compensated, which is caused by the addition of composite OMMT and the fusion of organic groups in epoxy resin. As shown in Figure 4b, when the amount of OMMT is 3%, the surface morphology of the composite coating is greatly improved compared with that of epoxy resin. As shown in Figure 4c, when the amount of OMMT is increased to 7%, the surface of OMMT aggregates, which may be caused by the excessive addition of OMMT and the saturation of its fusion with epoxy resin, and the roughness is not greatly improved.

In order to determine the effect of fillers on the surface roughness of epoxy resins, the AFMs of EP coatings and OMMT/EP composite coatings containing 3% and 7% OMMT were determined, respectively. Figure 4d–f show that the surface roughness of the EP coating is 65.5 nm, and the surface roughness of the OMMT/EP composite coatings with 3% and 7% OMMT, respectively, is smaller than that of the EP coating. The composite coatings with 7% OMMT addition are less rough, but there is agglomeration, which is consistent with the results of the surface morphology of the composite coatings mentioned

above. The results show that the addition of filler reduces the defects on the surface of the coating and the coating becomes smoother, which helps to prevent the intrusion of corrosive ions, but it is not better to add more.

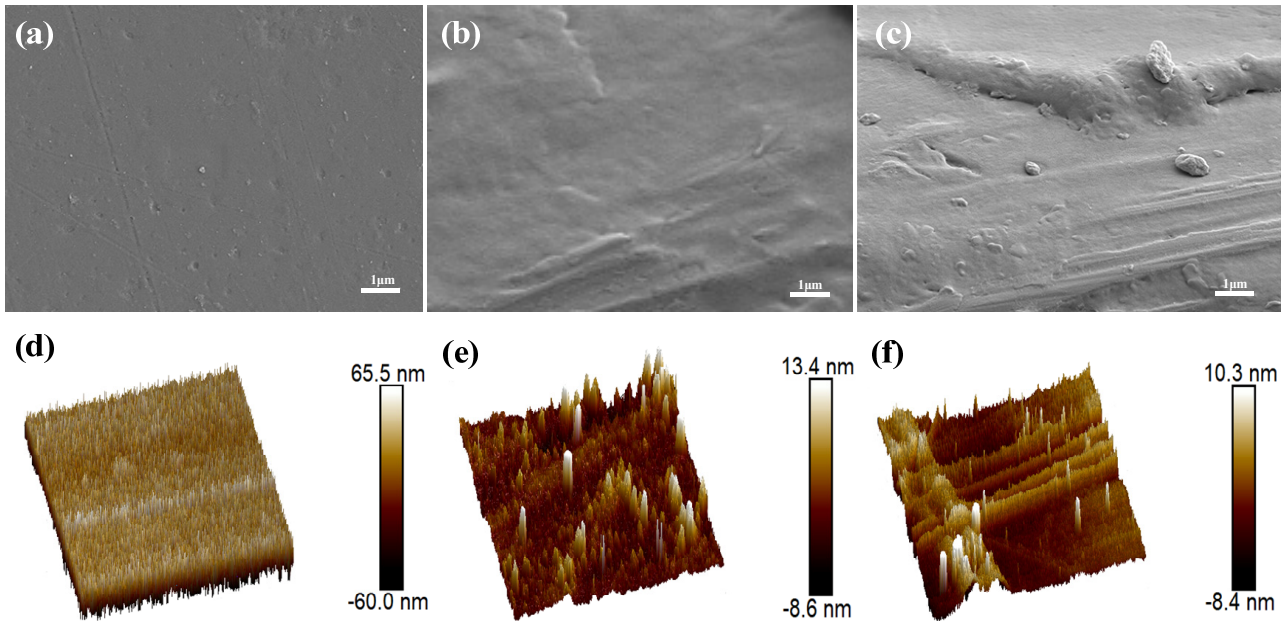


**Figure 4.** SEM images of (a) EP, (b) 3% OMMT/EP, and (c) 7% OMMT/EP; AFM diagram of (d) EP, (e) 3% OMMT/EP, and (f) 7% OMMT/EP.

### 3.4. Study on Corrosion Resistance of OMMT/EP Composite Coating

#### 3.4.1. Results and Analysis of the Polarization Curve

Tafel polarization curves of the OMMT/EP composite coating in solutions containing sodium sulfaluminate containing 5 g/L  $S^{2-}$  and 5 g/L  $S_2O_3^{2-}$  for the composite coating's thickness and time are shown in Figure 5. The values of corrosion current ( $I_{corr}$ ), corrosion potential ( $E_{corr}$ ), and polarization resistance ( $R_p$ ) obtained by fitting the polarization curves are shown in Tables 1 and 2.

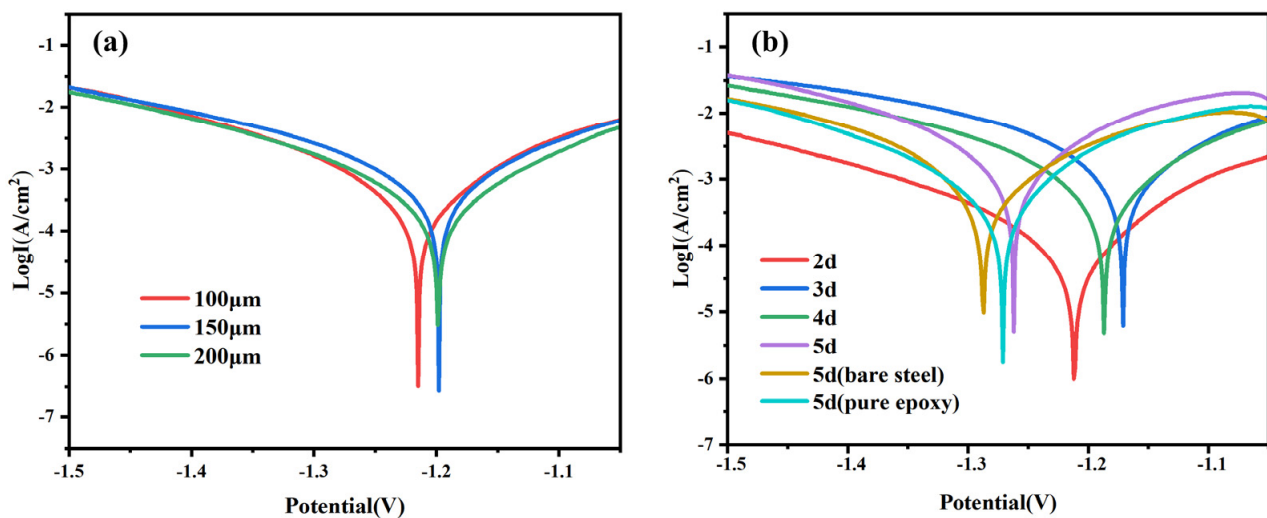


**Figure 5.** Polarization curves of composite coating with (a) different thicknesses and (b) different times.

**Table 1.** Polarization curve corrosion parameters of OMMT/EP composite coating thickness.

Coating Thickness/ $\mu\text{m}$	Corrosion Current ( $\text{A}\cdot\text{cm}^{-2}$ )	Corrosion Potential (V)	$\beta_a$	$\beta_b$	$R_p$ ( $\Omega/\text{cm}^{-2}$ )
100	$2.356 \times 10^{-4}$	−1.215	8.350	9.527	103.2
150	$2.342 \times 10^{-4}$	−1.198	7.472	7.995	104.6
200	$2.334 \times 10^{-4}$	−1.199	7.997	9.359	107.3

**Table 2.** Polarization curve corrosion parameters of OMMT/EP composite coating time.

Soak Time/d	Corrosion Current ( $\text{A}\cdot\text{cm}^{-2}$ )	Corrosion Potential (V)	$\beta_a$	$\beta_b$	$R_p$ ( $\Omega/\text{cm}^{-2}$ )	$P_E\%$
2	$6.695 \times 10^{-4}$	−1.212	7.690	10.475	357.5	-
3	$1.198 \times 10^{-3}$	−1.171	6.467	7.626	168.7	-
4	$5.791 \times 10^{-4}$	−1.187	7.209	8.347	130.3	-
5	$1.551 \times 10^{-4}$	−1.262	7.203	7.641	120.5	77.90
5 (bare steel)	$7.017 \times 10^{-4}$	−1.287	7.274	7.722	41.3	-
5 (pure epoxy)	$4.823 \times 10^{-4}$	−1.271	7.870	8.286	55.8	31.27

The calculation of  $R_p$  from the Stern–Geary equation [26–28]:

$$R_p = \frac{\beta_a \beta_b}{2.303(\beta_a + \beta_b)I_{\text{corr}}} \quad (1)$$

where  $I_{\text{corr}}$  is determined by the intersection of the anodic and cathodic linear portions of the polarization curve, and  $\beta_a$  and  $\beta_b$  are the Tafel slopes of the anode and cathode of the sample, respectively.

In order to better investigate the strength of the coating's corrosion resistance, the corrosion resistance of the coating can be characterized in terms of the protection efficiency ( $P_E$ ).

$$P_E\% = \frac{I_{\text{corr}}(\text{uncoated}) - I_{\text{corr}}(\text{coated})}{I_{\text{corr}}(\text{uncoated})} \times 100\% \quad (2)$$

The characteristics of the cathodic sections in Figure 5a,b are the same, indicating that the thickness and time do not have much effect on the cathodic process. At the same time, the anodic curves show different patterns of change. The smaller the  $I_{\text{corr}}$ , the better the corrosion resistance of the coating [29]. Table 1 shown that the  $I_{\text{corr}}$  is relatively small at  $2.334 \times 10^{-4}$  for a thickness of 200  $\mu\text{m}$ , and its  $R_p$  is the maximum. From the  $I_{\text{corr}}$  and  $E_{\text{corr}}$ , the coating prepared in this study with a thickness of 200  $\mu\text{m}$  has a good barrier effect on the corrosion of Q235 steel.

Figure 5b and Table 2 show that the  $I_{\text{corr}}$  of the OMMT/EP composite coating is minimum at 3 d.  $R_p$  decreases with time slowly from the third day onwards [27]. After the OMMT/EP composite coatings, EP coatings and bare steel were immersed in the same environment for 5 d; the  $I_{\text{corr}}$  of the OMMT/EP composite coating was  $1.551 \times 10^{-4}$  minimum, and the protection efficiency was 77.90%, higher than that of EP coating. It is shown that incorporating OMMT filler can effectively improve the corrosion resistance of the coating. This is consistent with the SEM and AFM results.

### 3.4.2. Electrochemical Impedance Spectroscopy Results and Analysis of OMMT/EP Composite Coating

Electrochemical impedance plots of the OMMT/EP composite coating's thickness and time are shown in Figures 6 and 7.

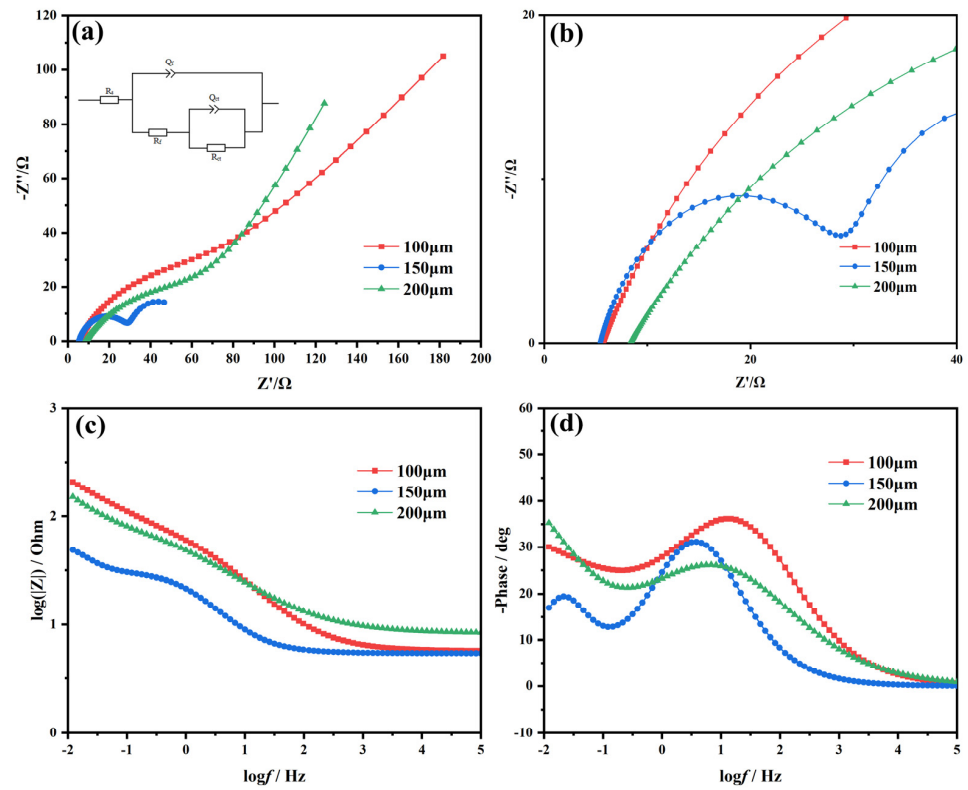


**Figure 6.** (a,b) Nyquist and (c,d) Bode plots of the thickness of OMMT/EP composite coating immersed in sulfur-containing sodium aluminum sulfate corrosive medium.

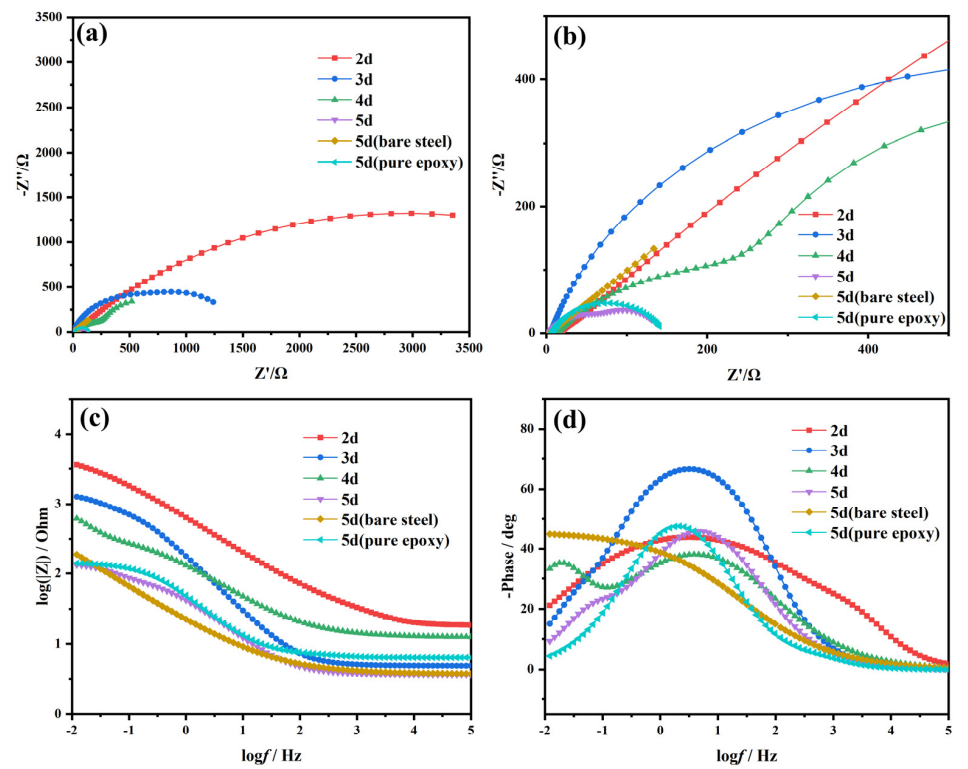


**Figure 7.** (a,b) Nyquist and (c,d) Bode plots of Q235 steels, EP, and OMMT/EP composite coating immersed in sulfur-containing sodium aluminum sulfate corrosive medium for a time.

As shown in Figure 6a,b, the larger the radius of the impedance arc, the higher the resistance of the coating and the better its anti-corrosion performance [30], where the impedance arc radius is largest for a thickness of 200  $\mu\text{m}$ . The mode value is larger in the lower-frequency region and becomes lower as the frequency increases, and the phase angle is larger in the higher-frequency region. It represents better corrosion protection of the coating [31]. The Bode plot shows that the phase angle of the coating thickness of 200  $\mu\text{m}$  is the largest, indicating that the anti-corrosion effect of the coating thickness of 200  $\mu\text{m}$  is better.

Figure 7a,b show that the impedance arc radius of the OMMT/EP composite coating is the largest on day three. With time, there is a decrease. Figure 7c,d show that the coated and uncoated steel sheets have the highest modal values in the low-frequency region. As the frequency increases, there is finally an impedance plateau in the high-frequency region and a certain phase angle in the mid-frequency region. Corrosion resistance decreases with time but not significantly [32]. The corrosion resistance of the OMMT/EP composite coating, EP coating, and Q235 steel has little effect when immersed in the corrosive medium for 5 d.

According to the equivalent circuit, Zview 3.1 software was used to fit the electrochemical impedance spectrum of the composite coating on the surface of Q235 steel. The relevant electrochemical parameters are shown in Tables 3 and 4.

**Table 3.** Electrochemical parameters of OMMT/EP composite coating with thicknesses.

Thickness	100 $\mu\text{m}$	150 $\mu\text{m}$	200 $\mu\text{m}$
$R_s/\Omega\cdot\text{cm}^{-2}$	5.6160	5.5	8.1110
$\text{CPE}_f(Y_0)/\Omega^{-1}\cdot\text{cm}^{-2}\cdot\text{s}^{-n}$	0.0029	0.0081	0.0061
$n_1$	0.6297	0.7635	0.4988
$R_f/\Omega\cdot\text{cm}^{-2}$	79.650	100.140	116.50
$\text{CPE}_{ct}(Y_0)/\Omega^{-1}\cdot\text{cm}^{-2}\cdot\text{s}^{-n}$	0.0201	0.2241	0.0064
$n_2$	0.4942	0.5152	0.4956
$R_{ct}/\Omega\cdot\text{cm}^{-2}$	$4.46 \times 10^{15}$	$1.039 \times 10^{14}$	$1.176 \times 10^{12}$

**Table 4.** Electrochemical parameters of OMMT/EP composite coating with times.

Sample	OMMT/EP				Bare Steel	Pure Epoxy
Time	2	3	4	5	5	5
$R_s/\Omega\cdot\text{cm}^{-2}$	18.42	4.956	12.45	3.638	3.791	6.498
$\text{CPE}_f(Y_0)/\Omega^{-1}\cdot\text{cm}^{-2}\cdot\text{s}^{-n}$	$1.51 \times 10^{-5}$	0.0012	0.0022	0.0049	0.0199	0.0003
$n_1$	0.8695	0.8210	0.5804	0.7144	0.5084	0.5124
$R_f/\Omega\cdot\text{cm}^{-2}$	580.05	520.77	401.8	389.76	1.133	1.0540
$\text{CPE}_{ct}(Y_0)/\Omega^{-1}\cdot\text{cm}^{-2}\cdot\text{s}^{-n}$	0.0005	0.0141	0.0183	0.0592	$1.057 \times 10^{-10}$	0.0044
$n_2$	0.5366	0.6235	0.7356	0.9564	0.8202	0.7461
$R_{ct}/\Omega\cdot\text{cm}^{-2}$	5846	376.3	755.5	48.12	$8.433 \times 10^6$	138.4

#### 4. Conclusions

1. We successfully modified MMT with HDA to prepare OMMT, which reduced the polarity and surface energy of MMT, increased the layer spacing to 2.87 nm, and greatly improved the hydrophobicity, which provided the basis for the preparation of composite coatings.
2. Adding filler into the OMMT/EP composite coating results in a smoother surface than pure EP coating, reducing surface defects. This smooth and flat surface is beneficial for preventing the infiltration of corrosive ions in the corrosion solution. The best performance of the 7% OMMT/EP composite coating was verified by surface morphology and roughness tests.

3. The corrosion resistance of the OMMT/EP composite coating demonstrates a decrease in  $I_{\text{corr}}$  and an increase in impedance value with increasing thickness of the composite coating. However, with increasing soaking time, minimal change is observed in both the  $I_{\text{corr}}$  and impedance values. Notably, after 5 days of soaking, the EP coating exhibited a protection rate of 31.27%, whereas the composite coating showed an enhanced protection efficiency of 77.90%.

**Author Contributions:** Conceptualization, J.X.; Validation, D.L.; Investigation, J.X.; Resources, B.Q.; Data curation, J.X.; Writing—original draft, J.X.; Writing—review & editing, H.W.; Supervision, B.Q.; Project administration, B.Q. All authors have read and agreed to the published version of the manuscript.

**Funding:** This research was funded by National Natural Science Foundation of China, No. U1812402 and Guizhou university talent introduction project, No. [2020]43.

**Institutional Review Board Statement:** Not applicable.

**Informed Consent Statement:** Not applicable.

**Data Availability Statement:** Data are contained within the article.

**Conflicts of Interest:** The authors declare no conflicts of interest.

## References

1. Chen, M.; Gai, J.X.; Chen, C.Y.; Li, J.Q. Corrosion evolution of 15CrMn steel in sulfur-containing sodium aluminate solution. *Mater. Lett.* **2022**, *310*, 131464. [[CrossRef](#)]
2. Fu, H.; Chen, C.Y.; Li, J.Q.; Lan, Y.P.; Wang, L.Z.; Yuan, J.J. Influence of  $\text{Na}_2\text{S}$  on the corrosion behavior of Q345 steel in sodium aluminate solution. *Mater. Res. Express* **2019**, *6*, 1065a9. [[CrossRef](#)]
3. Hu, X.L.; Chen, W.M. Study of sulfur removal from sodium aluminate solution using wet oxidation method. *J. Cent. South Univ. Nat. Sci. Ed.* **2011**, *42*, 2911–2916.
4. Yang, X.-Q.; Chen, C.-Y.; Li, J.-Q.; Quan, B.-L. A review of research on alkal-ine corrosion of steel by sulfur. *Surf. Technol.* **2015**, *44*, 89–95.
5. Du, X.-Y.; Yin, Y.-Y.; Liu, C.-M.; Dong, Y.-H.; Zhang, H.-B.; Qiu, P. Preparation of MXene@PAIN composites and their application in epoxy coatings. *Coat. Ind.* **2023**, *53*, 16–22+26.
6. Zhang, X.L.; Li, B.; Chen, T.T.; Xiang, K.; Xiao, R.G. Study on  $\text{CePO}_4$  modified PANI/RGO composites to enhance the anti-corrosion property of epoxy resin. *Prog. Org. Coat.* **2023**, *178*, 107472. [[CrossRef](#)]
7. Liu, W.L.; Li, J.S. Sodium Lignosulfonate-Loaded Halloysite Nanotubes/Epoxy Composites for Corrosion Resistance Coating. *ACS Omega* **2023**, *8*, 18425–18434. [[CrossRef](#)] [[PubMed](#)]
8. Liu, J.Y.; Wu, S.Z.; Shen, Z.; Gao, J.; Hu, X.Q.; Li, G.H. Enhanced anticorrosion property of epoxy resin membrane by nano-organic montmorillonite. *J. Coat. Technol. Res.* **2022**, *19*, 1087–1100. [[CrossRef](#)]
9. Wang, S.; Hu, Z.R.; Shi, J.; Chen, G.K.; Zhang, Q.; Weng, Z.S.; Wu, K.; Lu, M. Green s-synthesis of graphene with the assistance of modified lignin and its application in anticorrosive waterborne epoxy coatings. *Appl. Surf. Sci.* **2019**, *484*, 759–770. [[CrossRef](#)]
10. Shi, X.; Nguyen, T.A.; Suo, Z.; Liu, Y.; Avci, R. Effect of nanoparticles on the anticorrosion and mechanical properties of epoxy coating. *Surf. Coat. Technol.* **2009**, *204*, 237–245. [[CrossRef](#)]
11. Park, J.; Jane, S.C. Effect of plasticization of epoxy networks by organic modifier on exfoliation of nanoclay. *Macromolecules* **2003**, *36*, 8391–8397. [[CrossRef](#)]
12. Park, S.J.; Kim, B.J.; Seo, D.I.; Rhee, K.Y.; Lyu, Y.Y. Effects of a silane treatment on the mechanical interfacial properties of montmorillonite/epoxy nanocomposites. *Mater. Sci. Eng. A* **2009**, *526*, 74–78. [[CrossRef](#)]
13. Rodlert, M.; Plummer, C.J.G.; Leterrier, Y.; Manson, J.-A.E.; Grünbauer, H.J.M. Rheological behavior of hyperbranched polymer/montmorillonite clay nanocomposites. *J. Rheol.* **2004**, *48*, 1049–1065. [[CrossRef](#)]
14. Sari, M.G.; Ramezanzadeh, B.; Shahbazi, M.; Pakdel, A. Influence of nanoclay particles modification by polyester-amide hyperbranched polymer on the corrosion protective performance of the epoxy nanocomposite. *Corros. Sci.* **2015**, *92*, 162–172. [[CrossRef](#)]
15. Li, J.; Ecco, L.; Fedel, M.; Ermini, V.; Delmas, G.; Pan, J. In-Situ AFM and EIS study of a solventborne alkyd coating with nanoclay for corrosion protection of carbon steel. *Prog. Org. Coat.* **2015**, *87*, 179–188. [[CrossRef](#)]
16. Jiang, F.W.; Zhao, W.J.; Wu, Y.M.; Wu, Y.H.; Liu, G.; Dong, J.D.; Zhou, K.H. A polyethyleneimine-grafted graphene oxide hybrid nanomaterial: Synthesis and anti-corrosion applications. *Appl. Surf. Sci.* **2019**, *479*, 963–973. [[CrossRef](#)]
17. Hua, Q.X.; Jing, B.; He, M.Y.; Sun, P.F.; Zhao, Q.; Su, S.L.; Hu, G.J.; Ping, D.H.; Li, S.J. Preparation of modified montmorillonite/graphene oxide composites to enhance the anticorrosive performance of epoxy coatings. *J. Coat. Technol. Res.* **2023**, *20*, 1111–1119. [[CrossRef](#)]

18. Mohammadzadeh, A.; Taleghani, H.G.; Lashkenari, M.S. Preparation and comparative study of anticorrosion nanocomposites of polyaniline/graphene oxide/clay coating. *J. Mater. Res. Technol.* **2021**, *13*, 2325–2335. [[CrossRef](#)]
19. Zhou, Y.; Wang, H.R.; Zhang, C.; Zhou, Q.X.; Rodrigues, D.F. Graphene Oxide-Hybridized Waterborne Epoxy Coating for Simultaneous Anticorrosive and Antibiofilm Functions. *Front. Mater.* **2022**, *9*, 910152. [[CrossRef](#)]
20. Merachtsaki, D.; Xidas, P.; Giannakoudakis, P.; Triantafyllidis, K.; Spathis, P. Corrosion Protection of Steel by Epoxy-Organoclay Nanocomposite Coatings. *Coatings* **2017**, *7*, 84. [[CrossRef](#)]
21. De Paula, A.S.; Aroeira, B.M.; Souza, L.H.d.O.; da Cruz, A.C.; Fedel, M.; Da Silva, B.P.; Cotting, F. Influence of Organic Coating Thickness on Electrochemical Impedance Spectroscopy Response. *Coatings* **2024**, *14*, 285. [[CrossRef](#)]
22. Chen, Y.; Bai, W.; Chen, J.; Chen, X.; Zhao, J.; Wei, F.; Jian, R.; Zheng, X.; Xu, Y. In-Situ intercalation of montmorillonite/urushiol titanium polymer nanocomposite for anti-corrosion and anti-aging of epoxy coatings. *Prog. Org. Coat.* **2022**, *165*, 106738. [[CrossRef](#)]
23. Sadawy, M.M.; Fayed, S.M.; Tayea, M.; El-Batanony, I.G. Microstructure, Corrosion and Electrochemical Properties of Cu/SiC Composites in 3.5 wt% NaCl Solution. *Met. Mater. Int.* **2023**, *30*, 568–584. [[CrossRef](#)]
24. Zhu, J.; Zhang, P.; Qing, Y.; Wen, K.; Su, X.; Ma, L.; Wei, J.; Liu, H.; He, H.; Xi, Y. Novel intercalation mechanism of zwitterionic surfactant modified montmorillonites. *Appl. Clay Sci.* **2017**, *141*, 265–271. [[CrossRef](#)]
25. Zhang, L.; Yu, W.; Han, C.; Guo, J.; Zhang, Q.; Xie, H.; Shao, Q.; Sun, Z.; Guo, Z. Large Scaled Synthesis of Heterostructured Electrospun TiO<sub>2</sub>/SnO<sub>2</sub> Nanofibers with an Enhanced Photocatalytic Activity. *J. Electrochem. Soc.* **2017**, *164*, H651–H656. [[CrossRef](#)]
26. Ledwig, P.; Ratajski, T.; Indyka, P.; Kalembe-Rec, I.; Kopia, A.; Kaç, M.; Dubiel, B. Microstructure and Properties of Electrodeposited nc-TiO<sub>2</sub>/Ni-Fe and Ni-Fe Coatings. *Met. Mater. Int.* **2020**, *26*, 812–826. [[CrossRef](#)]
27. Zhang, L.; Qin, M.; Yu, W.; Zhang, Q.; Xie, H.; Sun, Z.; Shao, Q.; Guo, X.; Hao, L.; Zheng, Y.; et al. Heterostructured TiO<sub>2</sub>/WO<sub>3</sub> nanocomposites for photocatalytic degradation of toluene under visible light. *J. Electrochem. Soc.* **2017**, *164*, 1086–1090. [[CrossRef](#)]
28. Sou, W.-F.; Fan, Y.-H.; Fu, J.-W. PPy/rGO composite coatings on aluminum alloys for aircraft structures and their anti-corrosion properties. *China Surf. Eng.* **2019**, *32*, 103–110.
29. Nie, M.; Huang, F.; Wang, Z.-G. Electrochemical synthesis of polypyrrole/poly-dopamine and its effect on the corrosion resistance of aluminum alloys. *J. Compos. Mater.* **2019**, *36*, 2364–2370.
30. Masumi, S.; Mahdavi, S.; Etmnanfar, M.R. Electrochemical deposition of bilayer PPy/PPy-HA coating on AZ31 Mg alloy: Effect of HA content on characteristics and corrosion protection. *Mater. Today Commun.* **2023**, *37*, 107034. [[CrossRef](#)]
31. Wu, L.K.; Zhang, X.F.; Hu, J.M. Corrosion protection of mild steel by one-step electrodeposition of superhydrophobic silica film. *Corros. Sci.* **2014**, *85*, 77–482. [[CrossRef](#)]
32. Monteiro, R.D.; van de Wetering, J.; Krawczyk, B.; Engelberg, D.L. Corrosion Behaviour of Type 316L Stainless Steel in Hot Caustic Aqueous Environments. *Met. Mater. Int.* **2020**, *26*, 630–640. [[CrossRef](#)]

**Disclaimer/Publisher’s Note:** The statements, opinions and data contained in all publications are solely those of the individual author(s) and contributor(s) and not of MDPI and/or the editor(s). MDPI and/or the editor(s) disclaim responsibility for any injury to people or property resulting from any ideas, methods, instructions or products referred to in the content.